MBoC | ARTICLE

KLP-7/Kinesin-13 orchestrates axon-dendrite checkpoints for polarized trafficking in neurons

Swagata Dey[a,*], Nitish Kumar[a,‡], Supraja Balakrishnan[a], Sandhya P. Koushika[b], and Anindya Ghosh-Roy[a,*]

[a]Cellular and Molecular Neuroscience, National Brain Research Centre, Manesar, Gurugram, Haryana 122052, India; [b]Department of Biological Sciences, Tata Institute of Fundamental Research, Mumbai, Maharashtra 400005, India

ABSTRACT **The polarized nature of neurons depends on their microtubule dynamics and orientation determined by both microtubule-stabilizing and destabilizing factors. The role of destabilizing factors in developing and maintaining neuronal polarity is unclear. We investigated the function of KLP-7, a microtubule depolymerizing motor of the Kinesin-13 family, in axon-dendrite compartmentalization using PVD neurons in *Caenorhabditis elegans*. Loss of KLP-7 caused a mislocalization of axonal proteins, including RAB-3, SAD-1, and their motor UNC-104, to dendrites. This is rescued by cell-autonomous expression of the KLP-7 or colchicine treatment, indicating the involvement of KLP-7-dependent microtubule depolymerization. The high mobility of KLP-7 is correlated to increased microtubule dynamics in the dendrites, which restricts the enrichment of UNC-44, an integral component of Axon Initial Segment (AIS) in these processes. Due to the loss of KLP-7, ectopic enrichment of UNC-44 in the dendrite potentially redirects axonal traffic into dendrites that include plus-end out microtubules, axonal motors, and cargoes. These observations indicate that KLP-7-mediated depolymerization defines the microtubule dynamics conducive to the specific enrichment of AIS components in dendrites. This further compartmentalizes dendritic and axonal microtubules, motors, and cargoes, thereby influencing neuronal polarity.**

SIGNIFICANCE STATEMENT

- Neuronal polarization ensures distinct compartmentalization of molecules within the neuron and is required for its proper function. It is unclear how microtubule destabilization factors participate in the process.
- Using PVD neurons in *C. elegans*, the authors establish that KLP-7 (Kinesin-13) specifically regulates axon-dendrite compartmentalization. KLP-7-dependent microtubule depolymerization limits the formation of the axon initial segment (AIS), preventing the entry of axonal molecules into the dendrites.
- The study advances the understanding of how cytoskeletal regulators define compartmentalization in neurons required for the maintenance of the molecular repertoire of neurites and their identity.

Monitoring Editor
Stephanie Gupton
University of North Carolina at Chapel Hill

Received: Sep 5, 2023
Revised: Jun 27, 2024
Accepted: Jul 3, 2024

New Hypothesis

This article was published online ahead of print in MBoC in Press (http://www.molbiolcell.org/cgi/doi/10.1091/mbc.E23-08-0335) on July 10, 2024.

Conflict of interests: The authors declare no competing financial interests.

Author contributions: S.D., and A.G-R designed experiments. S.D., and N.K. performed experiments and analyzed data. S.B. helped in crossing strains and making reagents. S.P.K. provided reagent and helped in data interpretation and discussion. S.D. and A.G-R wrote and edited the manuscript.

†Present addresses: Huck Institutes of Life Sciences, Pennsylvania State University, PA 16802.

*Address correspondence to: Swagata Dey (swagatad86@nbrc.ac.in); Anindya Ghosh-Roy (anindya@nbrc.ac.in).

Abbreviations used: AIS, axon initial segment; ANOVA, analysis of variance; BAR, broadly applicable routines plugin; CGC, *Caenorhabditis elegans* center; CLASP, cytoplasmic linker-associated proteins; CRISPR, clustered regularly interspaced short palindromic repeats; CRMP2, collapsin response mediator protein 2; DBT, department of biotechnology; DMA-1, dendrite morphology abnormal-1; EBP-2, end binding protein-2; EFA-6, exchange factor for Arf-6; FRAP, fluorescence recovery after photobleaching; GFP, green fluorescent protein; IA, India Alliance; KIF2, kinesin family member 2; KLP-7, kinesin-like protein-7; Klp10, kinesin like protein 10; MAP2C, microtubule associated protein 2C; MCAK, mitotic centromere-associated kinesin; Msps, mini spindles; NBRC, National Brain Research Centre; NGM, nematode growth medium; NIH, National Institute of Health; NOCA-2, Non-centrosomal microtubule array-2; Op18, oncoprotein 18; PLM, posterior lateral microtubule neuron; PTRN-1, patronin homolog-1; PVD, posterior ventral process D; RAB-3, Ras-associated binding homolog-3; ROI, Region of Interest; SAD-1, synapses of amphid defective-1; SNT, simple neurite tracer; TIAM-1, tumor invasion and metastasis factor homolog-1; TRIM46, tripartite motif containing 46; UNC-104, uncoordinated-104; UNC-119, uncoordinated-119; UNC-33, uncoordinated-33; UNC-44, Uncoordinated-44.

INTRODUCTION

The polarized structure and composition of the neurons enable directional information transfer in a neural circuit. Microtubules are one of the crucial determiners of neuronal polarization (Barnes and Polleux, 2009; Marín *et al.*, 2010; Kuijpers and Hoogenraad, 2011; Yogev and Shen, 2017). Dynamics and organization of microtubules define neuronal migration, selective intracellular trafficking, organelle positioning, signaling hubs, and force generators in the developing neurons (Tolić-Nørrelykke, 2008; Hirokawa *et al.*, 2010; De Forges *et al.*, 2012; Subramanian and Kapoor, 2012). Microtubules are made of α and β tubulin heterodimers equilibrating between phases of polymerization and depolymerization that define their polarity, dynamics, and organization during neuronal morphogenesis (Sakakibara *et al.*, 2013; Horio *et al.*, 2014; Kapitein and Hoogenraad, 2015; Kelliher *et al.*, 2019; Gudimchuk and McIntosh, 2021).

In the context of neuronal polarity, regulators of microtubule stabilization have been well investigated (Baas *et al.*, 1991, 2016; Witte *et al.*, 2008; Polleux and Snider, 2010) for example, MAP2C and TRIM46 stabilize the microtubule array and are important for the axon initiation (Dehmelt *et al.*, 2006; Van Beuningen *et al.*, 2015). Similarly, microtubule assembly regulator Collapsin Response Mediator Protein 2 (CRMP2) regulates the compartmentalization of axons and dendrites (Arimura *et al.*, 2004; Yoshimura *et al.*, 2005; Maniar *et al.*, 2012). Microtubule destabilizers like Stathmin/Op18 are locally inactivated in the nascent axon during development (Watabe-Uchida *et al.*, 2006). Similarly, a microtubule severing protein, Katanin is finely regulated for the proper axon development (Karabay *et al.*, 2004; Yu *et al.*, 2005; Qiang *et al.*, 2006). Conditional loss of microtubule depolymerizing KIF2/Kinesin-13 in the rodent hippocampus and KLP-7 in *Caenorhabditis elegans* caused the formation of ectopic branches and loss of axon-dendrite compartmentalization (Homma *et al.*, 2003, 2018; Ghosh-Roy *et al.*, 2012; Puri *et al.*, 2021). The roles and mechanisms of microtubule depolymerizers in the process of neuronal polarization are yet to be investigated in detail.

PVD neurons are highly polarized neurons with a well-defined axon and highly stereotyped dendritic arbor. These are mechanosensory neurons for proprioception, harsh touch, and cold temperature sensation (Way and Chalfie, 1989; Chatzigeorgiou *et al.*, 2010; Albeg *et al.*, 2011; Brar *et al.*, 2024). Previous studies have elucidated the role of various regulators, including Ankyrin (UNC-44), CRMP2 (UNC-33), UNC-119, Patronin (PTRN-1), Ninein (NOCA-2), and TIAM-1 in the process of neuronal polarity (Maniar *et al.*, 2012; He *et al.*, 2020, 2022; Lin *et al.*, 2022). Loss of function of these genes caused aberrant microtubule organization and mislocalization of the axonal cargoes into the dendrites (Maniar *et al.*, 2012; He *et al.*, 2020, 2022; Lin *et al.*, 2022). It is unclear how microtubule depolymerizing factors such as KLP-7 or EFA-6 influence axon-dendrite compartmentalization.

In this study, we have found a specific role of KLP-7/Kinesin-13 in the proper compartmentalization of axons and dendrites in the PVD neurons. Using a reporter of microtubule dynamics, EBP-2::GFP, we have found that KLP-7 maintains an increased level of microtubule dynamics and minus-end-out microtubule organization in the major dendrite of the PVD neuron. In the absence of KLP-7, the axonal cargoes, including RAB-3, SAD-1, and the motor UNC-104 populate the dendrites. This correlates with decreased microtubule dynamics, increased population of plus-end-out microtubules, and ectopic accumulation of the AIS component UNC-44 in dendrites. Our study suggests that KLP-7 optimizes microtubule dynamics in PVD neurites critical to preventing ectopic enrichment of AIS components in the dendrites.

RESULTS

KLP-7/Kinesin-13 regulates the axon-dendrite compartmentalization in the PVD neurons

KLP-7 is a motor of the Kinesin-13 family required for the dynamic instability of the microtubules through depolymerization (Desai *et al.*, 1999; Srayko *et al.*, 2005; Trofimova *et al.*, 2018). Human orthologue of KLP-7, KIF2 has been associated with clinical manifestations of cortical development, epilepsy, microcephaly, and Autism Spectrum Disorder (Poirier *et al.*, 2013; Yuen *et al.*, 2015; Tian *et al.*, 2016; Cavallin *et al.*, 2017; Costain *et al.*, 2019). Conditional knockout of KIF2 in rodents resulted in defects in neuritogenesis, neuronal maturation, function, and survival (Ogawa and Hirokawa, 2015; Homma *et al.*, 2018; Ruiz-Reig *et al.*, 2022). Similar anatomical defects were also observed in the touch neurons of *C. elegans*, where the loss of the *klp-7* gene resulted in the formation of ectopic neurites with axonal markers (Puri *et al.*, 2021). The mechanism by which Kinesin-13 regulates the axonal and dendritic identities is not clear.

We investigated aspects of neuronal polarity in the loss of function mutant of *klp-7* (Kinesin-13). We checked the distribution of the axonal marker, RAB-3 as a reporter for neuronal polarity in the PVD neuron (Figure 1A). PVD neurons of *C. elegans* have a well-defined axon running ventrally and fasciculated with the ventral nerve cord and a highly stereotyped dendritic arbor with orthogonal branches (Albeg *et al.*, 2011; Sundararajan *et al.*, 2019). The mCherry::RAB-3 reporter appears punctate mostly in the ventral nerve cord region in the control (wildtype) background (Figure 1A). Unlike in wildtype, mCherry::RAB-3 was also present in the dendrites of the *klp-7* null mutant (Figure 1B-C). Estimation of the dendritic branches containing mCherry::RAB-3 showed an accumulation in 11.5% of the dendritic branches of *klp-7(0)* as compared with 3.5% in the wildtype (Figure 1D). Though the loss of *klp-7* caused localization of mCherry::RAB-3 throughout the PVD neuron, including the minor dendrite, it was more pronounced in the distal region of the major dendrite where *klp-7* null mutant had ~29% dendrites with mCherry::RAB-3 as compared with 11.8% of the wildtype (Supplemental Figure S1A). This accumulation was prominent in the tertiary branches of *klp-7(0)* with 33.2% occupancy (Supplemental Figure S1B). Interestingly, quaternary branches of the *klp-7* null mutant also showed mislocalization of mCherry::RAB-3 (Supplemental Figure S1B). Moreover, the precedence of mCherry::RAB-3 in the dendrites as observed by the relative density and intensity of these particles, was also increased in the null mutant of *klp-7* (Figure 1, E and F). Though *klp-7* mutant dendrites showed remarkably increased occupancy by RAB-3 particles as observed by the intensity and density of the particles, the axons did not show any difference to the wildtype (Supplemental Figure S1, C and D). As we did not observe complete misrouting of RAB-3 to the dendrites, we speculate that higher accumulation in the dendrites may be because of an increased anterograde transport in the mutant.

As KLP-7 is a microtubule catastrophe factor, we asked whether any other microtubule-catastrophe factor would also regulate the axon-dendrite compartmentalization. We investigated another mutant that has a loss of function of *efa-6*. Apart from the conventional role in membrane trafficking and actin regulation (Franco *et al.*, 1999), in *C. elegans*, EFA-6 has a microtubule depolymerizing domain that causes the catastrophe of the microtubules near the cell cortex (O'Rourke *et al.*, 2010). Loss of EFA-6 causes the cells to have long microtubules and has been phenotypically correlated to spindle defects, embryonic lethality, and *dlk-1*-independent axon regeneration (O'Rourke *et al.*, 2010; Chen *et al.*, 2015; Qu *et al.*, 2019). Unlike the loss of function mutant of *klp-7*, a null mutant of *efa-6* did not mislocalize RAB-3 to the dendrites (Figure 1, B and C).

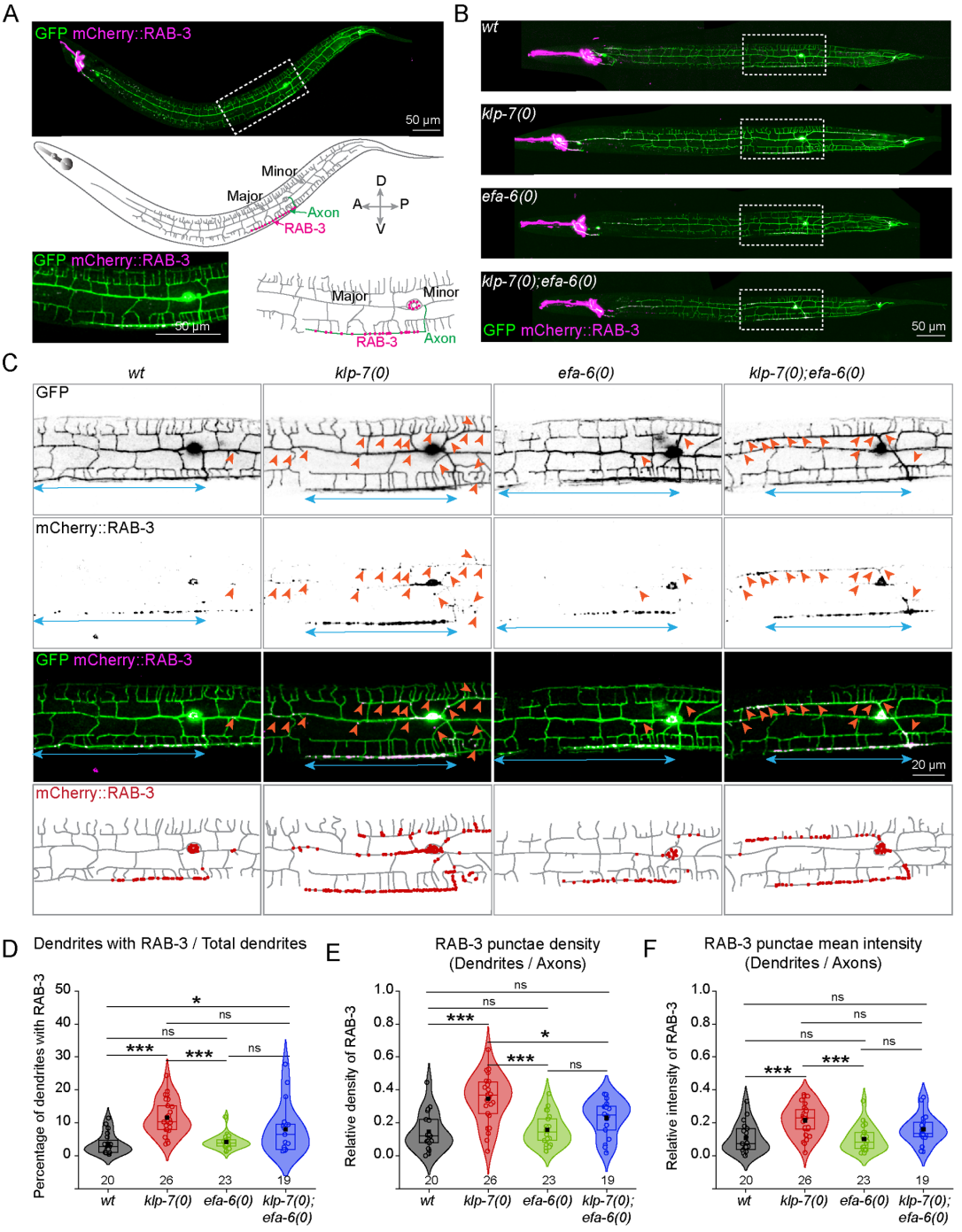

FIGURE 1: KLP-7 is required for the proper axon-dendrite compartmentalization in the PVD neurons. (A) Representative images and schematics of the PVD neuron expressing soluble GFP (green) and mCherry::RAB-3 (magenta), with the region around the cell body (dashed box) magnified below. Schematic depicts crosshair reference points of body symmetry (A- anterior, P- posterior, D- dorsal, V- ventral). (B and C) Representative images of the whole PVD neuron expressing soluble GFP (green) and mCherry::RAB-3 (magenta) in the wildtype (*wt*), and loss of function mutants of *klp-7(0)*, *efa-6(0)*, and double mutant of *klp-7(0)* and *efa-6(0)* with the regions around the cell body (dashed box) magnified and schematized in (C). The axonal and dendritic distributions of mCherry::RAB-3 in (C) are marked by the blue arrows and yellow arrowheads, respectively. Schematic in (C) shows the distribution of mCherry::RAB-3 (red dots) in the dendritic arbor of various mutants. (D) Quantification of the dendritic branches showing accumulation of mCherry::RAB-3 in the wildtype (*wt*), and loss of function mutants of *klp-7(0)*, *efa-6(0)*, and double mutant of *klp-7(0)* and *efa-6(0)* normalized to the total number of dendritic branches represented as a percentage. Comparison of means was done using ANOVA and Bonferroni Test. $p < 0.05$*, 0.001***, ns (not significant). Number of animals assessed (n) is mentioned along the X-axis. (E and F) Relative particle density (E) and mean intensity (F) of the particles of mCherry::RAB-3 quantified for the dendrites (major and minor) with respect to the axon of PVD neurons of wildtype (wt), *klp-7(0)*, *efa-6(0)*, and *klp-7(0);efa-6(0)* double mutant. Comparison of means within a category was done using ANOVA and Bonferroni Test and $p > 0.05$*, 0.001***. Number of worms assessed (n) is mentioned along the X- axis.

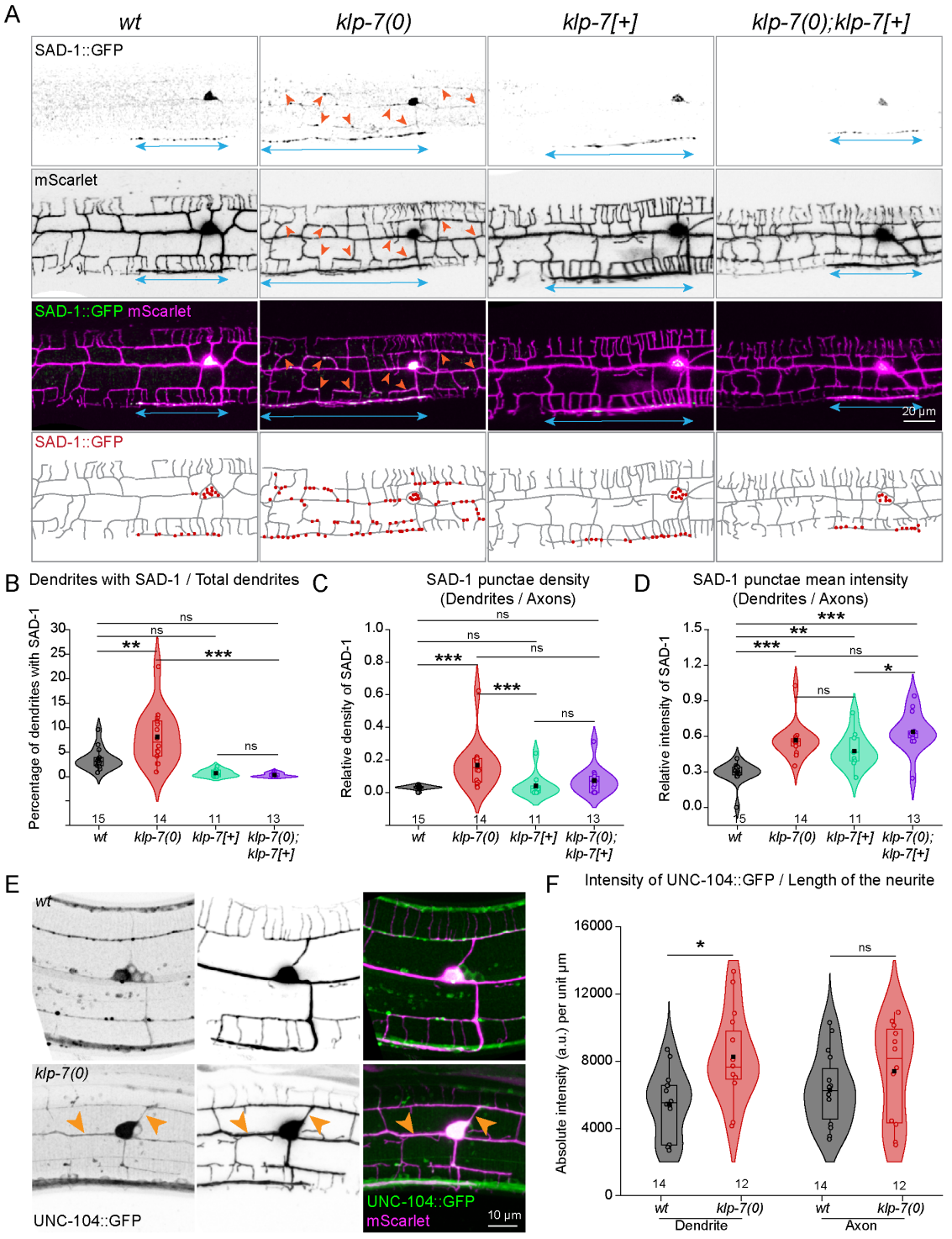

FIGURE 2: KLP-7 is necessary and sufficient to maintain polarized trafficking in the axons and dendrites.
(A) Representative images and schematics of PVD neuron expressing SAD-1::GFP (green) and mScarlet (magenta) in the wildtype (*wt*), and loss of function mutant of *klp-7(0)*, PVD specific overexpression of 15 ng *klp-7b* isoform (*klp-7[+]*), and PVD specific rescue of *klp-7(0)* labeled as *klp-7(0);klp-7[+]*. The axonal and dendritic distributions of SAD-1::GFP are marked by the blue arrows and yellow arrowheads, respectively. Schematic shows the distribution of SAD-1::GFP (red dots) in the dendritic arbor of various genotypes. (B) Quantification of the dendritic branches showing accumulation of SAD-1::GFP in the wildtype (*wt*), mutant *klp-7(0)*, *klp-7[+]* overexpression, and *klp-7(0);klp-7[+]* rescue normalized to the total number of dendritic branches represented as a percentage. Comparison of means was done using ANOVA and Bonferroni Test. $p < 0.01$**, 0.001***, ns (not significant). Number of animals assessed (n) is mentioned along the X-axis. (C and D) Relative particle density (C) and mean intensity (D) of the particles of SAD-1::GFP quantified for the dendrites (major and minor) with respect to the axon of PVD neurons of the wildtype (*wt*), mutant *klp-7(0)*, *klp-7[+]* overexpression, and *klp-7(0);klp-7[+]* rescue. Comparison of means within a category was done using ANOVA and Bonferroni Test and

Measurement of the number of dendrites with RAB-3 and distribution of RAB-3 in the primary dendrites of the PVD neuron of *efa-6(0)* were equivalent to those of wildtype (Figure 1, D–F; Supplemental Figure S1, A and B). The axon-dendrite distinction seems to be preserved in this mutant like the wildtype. Furthermore, we did not observe a synergism between *klp-7* and *efa-6* in the double mutant as compared with the *klp-7* mutant alone (Figure 1, B–F; Supplemental Figure S1, A–D). Only in the posterior dendrite (minor), the effect of *klp-7(0)* seemed suppressed by *efa-6(0)* in the density of RAB-3 particles, indicating a differential requirement of KLP-7 in PVD neurites (Figure 1D; Supplemental Figure S1, A and C). Although microtubule depolymerization by KLP-7 and EFA-6 in the dendrites could be mechanistically different, the role of KLP-7 in neuronal polarity is highly specific.

Cell-autonomous role of KLP-7 in maintaining selective traffic in axons and dendrites

We observed another presynaptic marker SAD-1 kinase, which is required for neuronal polarity and presynaptic development (Crump *et al.*, 2001). SAD-1::GFP was expressed as part of the same transgene as mCherry::RAB-3 (Maniar *et al.*, 2012). Similar to RAB-3, SAD-1 also appears punctate and enriched in the Ventral Nerve Cord region of the PVD neurons (Maniar *et al.*, 2012). Loss of *klp-7* also resulted in the mislocalization of SAD-1 to the PVD dendrites (Figure 2A). This mislocalization was observed in nearly 8% of the dendrites (Figure 2B). To further assess the role of KLP-7 in SAD-1 localization, we expressed the KLP-7 cDNA (15 ng) under the PVD-specific promoter as an extrachromosomal array transgene. PVD-specific expression of the KLP-7 in the wild-type background did not show any SAD-1 localization to the dendrites (Figure 2, A and B). However, in the mutant background, expression of this transgene rescued the SAD-1 mislocalization phenotype (Figure 2, A and B).

We also scored the density and intensity of SAD-1 particles in the dendrites and axons of PVD neurons. Overexpression of the *klp-7* transgene in the *klp7(0)* background partially restored the relative localization of SAD-1 in the dendrites with respect to the axons (Figure 2, C and D). The density and intensity of the dendritic SAD-1 particles were restored to the wildtype levels in the rescue of *klp-7(0)* (Supplemental Figure S2, A and B). Interestingly, due to the expression of *klp-7* transgene in either wildtype or *klp-7* mutant background, the density and mean intensity of the SAD-1 particles were drastically reduced in the axonal process (Supplemental Figure S2, A and B), possibly due to a disruption in its anterograde transport. This was strengthened by the live observation of mCherry::RAB-3 particles in PVD neurons of wild type and *klp-7(0)* worms. In the wild type, RAB-3 particles were present in the primary dendrites of a small proportion of animals. These particles were mobile, however, long-duration runs were not observed (Supplemental Movie S1). Interestingly, we observed a robust anterograde movement in the *klp-7(0)*, in the primary, secondary, and ectopic branches of PVD neurons (Supplemental Movie S2).

To understand how KLP-7 could be regulating the process, we investigated the motor UNC-104, which is required for the anterograde trafficking of presynaptic components, including RAB-3 and SAD-1 (Hall and Hedgecock, 1991; Yonekawa *et al.*, 1998; Maniar *et al.*, 2012). We observed UNC-104::GFP expressed under its endogenous promoter as a GFP knock-in transgene (Cong *et al.*, 2021). Due to its ubiquitous neuronal expression, UNC-104::GFP was observable in multiple neuronal processes, including motor neuron commissures and sublateral nerve cords (Zhou *et al.*, 2001; Kumar *et al.*, 2010; Li *et al.*, 2016; Cong *et al.*, 2021). Based on neurite traces generated from the constitutive PVD reporter, mScarlet, we analyzed the intensities of UNC-104::GFP in the dendrites of PVD neurons. In the loss of function mutant of *klp-7*, we observed a marked increase in the UNC-104::GFP intensity in the dendritic regions of the PVD neurons (Figure 2, E and F) while the axonal intensity remains unchanged. This correlates with the ubiquitous localization of SAD-1 or RAB-3 in the *klp-7(0)* mutant. This suggested that KLP-7 regulates the entry of axonal traffic into the dendrites through a predominantly axonal motor, thereby defining the checkpoint to segregate the axonal and dendritic proteins.

Increased microtubule stability due to loss of *klp-7* affects the axon-dendrite compartmentalization

Microtubule organization in the neurons is important for the differential trafficking of the cargoes in the axonal versus dendritic compartments (Kapitein *et al.*, 2010; Kapitein and Hoogenraad, 2011; Maeder *et al.*, 2014). Previous studies have established the causal effect of microtubule stabilization on axon specification by pharmacological perturbation of the microtubules through Paclitaxel to induce multiple neurites with axonal identity (Xiao *et al.*, 2006; Witte *et al.*, 2008). On the other hand, microtubule destabilizers like Nocodazole and Colchicine could reduce the formation of dendrite-like processes (Witte *et al.*, 2008; Puri *et al.*, 2021).

As we observed a cell-autonomous role of *klp-7* to restrict the entry of axonal cargoes such as SAD-1 or RAB-3 in the PVD dendrites, we speculated that loss of *klp-7* might have increased the stability of microtubules in dendrites, thereby routing the axonal motors and cargoes into the dendrites. To understand whether KLP-7 mediated microtubule instability defines the dendritic identity, we used pharmacological upregulation of microtubule instability by Colchicine. Previously, Colchicine exposure has been used to suppress the effects of microtubule-stabilizing mutations in *C. elegans* (Kirszenblat *et al.*, 2013; Puri *et al.*, 2021). We used a concentration of 1 mM Colchicine, which has been shown to affect the microtubule dynamics and function of the gentle touch receptor neurons (Chalfie and Thomson, 1982; Bounoutas *et al.*, 2011; Lockhead *et al.*, 2016; Puri *et al.*, 2021). In the *klp-7* loss of function mutant, the prevalence of RAB-3 in the dendrites decreased significantly with exposure to Colchicine (Figure 3, A–C). We observed a marked reduction in the RAB-3 occupancy in the proportion of dendrites as well as the localization of RAB-3 particles in *klp-7(0)* dendrites upon Colchicine treatment (Figure 3, B and C). This is likely due to a balance between Colchicine mediated microtubule depolymerization with respect to stabilized microtubules in *klp-7(0)* mutant. To further strengthen this, we exposed the wildtype worms

$p > 0.05$*, 0.01**, 0.001***. Number of worms assessed (n) is mentioned along the X- axis. (E and F) Representative images (E) and quantification (F) of the distribution of endogenously UNC-104::GFP (green) in the dendrites and axons of PVD neurons expressing mScarlet (magenta). Enrichment of UNC-104::GFP in the dendrites in (E) are marked by yellow arrowheads. Comparison of absolute intensities of UNC-104::GFP in the dendrites and axons per unit of their lengths was done between wildtype (*wt*) and mutant *klp-7(0)* using ANOVA and Bonferroni Test. $p < 0.05$*, ns (not significant). Number of worms assessed (n) is mentioned along the X- axis.

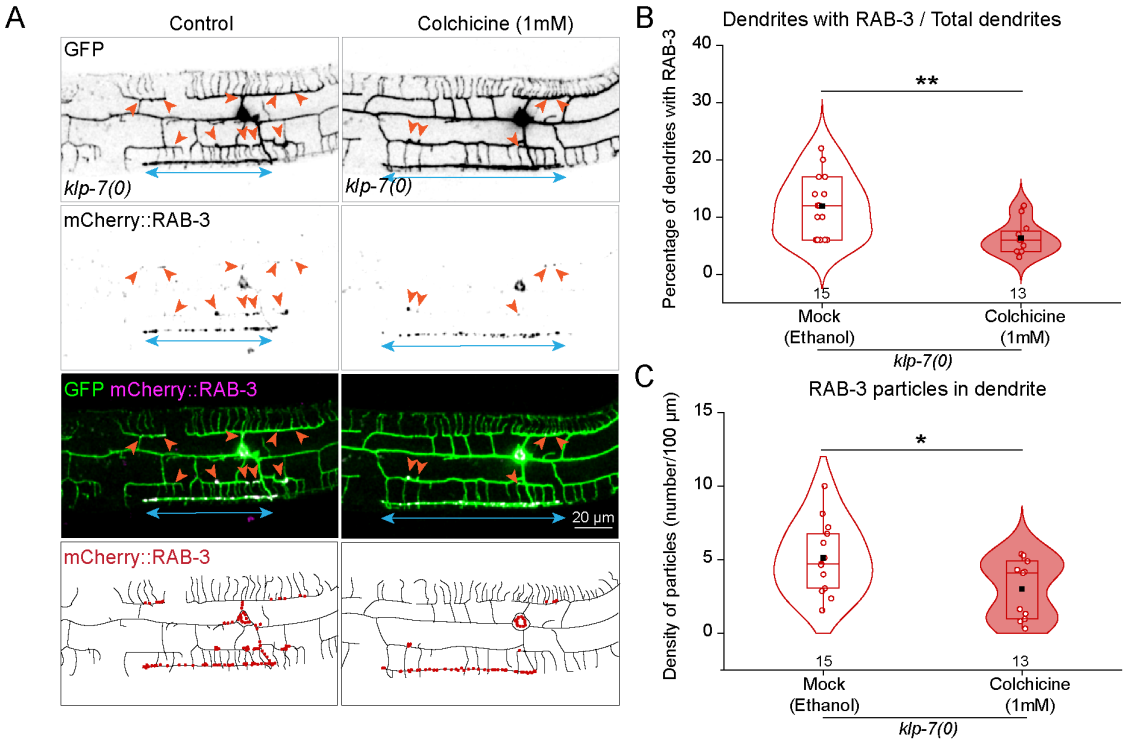

FIGURE 3: KLP-7-dependent microtubule organization defines the axon-dendrite compartmentalization. (A) Representative images of the *klp-7(0)* mutant following the treatment with Mock (Ethanol) and Colchicine (1 mM). The axonal and dendritic distributions of mCherry::RAB-3 are marked by the blue arrows and yellow arrowheads, respectively. Schematic shows the distribution of mCherry::RAB-3 (red dots) in the dendritic arbor of *klp-7(0)* upon Colchicine treatment. (B and C.) Percentage of the dendritic branches with respect to the total number of dendritic branches showing accumulation of mCherry::RAB-3 (B) and density of mCherry::RAB-3 particles in the primary dendrite (C) of the *klp-7(0)* mutant in mock and Colchicine treated conditions. Comparison of means was done using ANOVA and Bonferroni Test. $p < 0.05$*, 0.01**. Number of animals assessed (n) is mentioned along the X-axis.

to the same dose of Colchicine. As the dendrites of wildtype PVD neurons had negligible localization of RAB-3, Colchicine treatment did not alter this distribution (Supplemental Figure S3, A–C). However, the axonal distribution of RAB-3 particles in wildtype neurons was remarkably reduced upon Colchicine exposure (Supplemental Figure S3C). This suggested that KLP-7 maintains an optimal level of microtubule dynamics in the dendrites to prevent the entry of axonal cargoes like RAB-3 into dendrites.

Differential regulation of microtubule dynamics by Kinesin-13 is correlated to its mobility in neuronal compartments

Kinesin-13 is a key determinant of dynamic instability (Desai *et al.*, 1999; Srayko *et al.*, 2005; Ogawa *et al.*, 2017; Trofimova *et al.*, 2018). To understand the microtubule dynamics and organization regulated by KLP-7 in PVD neurons, we observed the dynamics of the plus tips of the microtubules using the EBP-2::GFP marker. EBP-2::GFP binds to the plus ends of microtubules and shows comet-like movement in a time-lapse acquisition (Stepanova *et al.*, 2003; Ghosh-Roy *et al.*, 2012). To assess the EBP-2::GFP dynamics, we generated the kymographs from segments (orange dotted lines) on the major and minor dendrites and axons of PVD neurons originating at the cell body (Figure 4A). In the kymographs, based on the angle, distance, and duration of the traces, polymerization rates and polarity were assessed (Figure 4A).

In the wild-type neurons, the rates of polymerization were higher in both the major and minor dendrites as compared with the axons (Figure 4, B and C), indicating higher microtubule dynamics in the dendrites. In the *klp-7(0)* mutant, not only the rates of polymerization were decreased globally, but also the distinction between the axon and dendrites became obsolete (Figure 4C). KLP-7 can affect the rates of polymerization by affecting the depolymerization on the microtubule plus ends and regulating the availability of α and β tubulin dimers for new polymerization events. Indirectly, other microtubule dynamics regulators like CLASP or loss of Mini Spindles (Msps) can accumulate on the plus ends (Li *et al.*, 2011; Moriwaki and Goshima, 2016) in the absence of Klp10-dependent depolymerization as observed for *Drosophila* microtubules can also participate in the process. Overexpression of the *klp-7* transgene also reduced the rates of polymerization in the dendrites, whereas in the *klp-7(0)* background, it rescued the rates of polymerization (Figure 4C). The major dendrite of both the *klp-7* overexpression *(klp-7[+])* and the rescue *(klp-7(0);klp-7[+])* showed higher dynamic microtubules than in the axons (Figure 4C). These results support that KLP-7-mediated depolymerization maintains the dynamic microtubules in the major dendrite of the PVD neurons.

We investigated the presence and mobility of GFP::KLP-7 in the major dendrite, minor dendrite, and the axon of the PVD neuron (Figure 4, D–F). Localization of GFP::KLP-7 was equivalent in all these compartments based on the normalized intensities (Figure 4D; Supplemental Figure S4A). Mobility of Kinesin-13/KLP-7 has been correlated to its activity in vitro and in the gentle touch neurons (Helenius *et al.*, 2006; Tan *et al.*, 2006; Puri *et al.*, 2021). Unlike other cargo-carrying motors, the mobility of Kinesin-13/ Mitotic Centromere-Associated Kinesin (MCAK)/ KLP-7 is not a direct readout of its depolymerization activity but its unidimensional diffusive

movement on the microtubule lattice (Helenius *et al*., 2006; Tan *et al*., 2006). However, Kinesin-13 mediated depolymerization is significantly facilitated by its movement on the microtubule lattice, indirectly correlating to its ability to scout and bind the microtubule ends for depolymerization (Helenius *et al*., 2006). Therefore, we assessed the mobility of GFP::KLP-7 in the primary dendrites and axon (Figure 4E) by Fluorescence Recovery After Photobleaching (FRAP) assay as an indirect readout of its activity in these compartments correlated with the differential microtubule dynamics. The FRAP assay revealed that the mobility of GFP::KLP-7 is significantly lesser in the axon with respect to the other compartments (Figure 4, E and F). Quantification of the maximum recovery from the recovery profiles showed a considerably small mobile fraction in the axon as compared with the major dendrite, and minor dendrite (Figure 4F). Moreover, a comparison of the halftimes of the recovery profiles also showed a delayed recovery in the AIS as compared with the major dendrite (Supplemental Figure S4, B and C). This is in line with the previous observations in wild-type PLM neurons where activity or mobility of KLP-7 was comparatively lower in the anterior process akin to the axon (Puri *et al*., 2021). The differential nature of KLP-7 in different compartments of the neuron allows these compartments to acquire a distinct microtubule organization (Puri *et al*., 2021).

Kinesin-13 regulates the relative orientation and distribution of dynamic microtubules in the major dendrite

Apart from microtubule dynamics, microtubule orientation is also a determiner of neuronal polarity or polarized trafficking in the neuron. The major dendrite showed minus end-out microtubules with the comets moving towards the cell body, whereas the minor dendrite and the axon showed plus end-out orientation of the microtubules (Figure 4B). This is similar to previous studies measuring the EBP-2::GFP comets in PVD neurons (Maniar *et al*., 2012; Harterink *et al*., 2018).

In the *klp-7(0)* mutant, the major dendrite showed a significant number of comets that are moving in the opposite direction as also visible in the kymographs (Figure 4B). We estimated the percentage of EBP-2::GFP comets in either direction for each kymograph. Based on the percentage of the EBP-2::GFP comets, the major dendrite of the wildtype had a minus end-out orientation of the microtubules, whereas the mutant has a mixed orientation (Figure 4G). On the other hand, *klp-7* loss of function did not perturb the plus end-out orientation of the microtubules in the minor dendrite or the axon (Figure 4, G–I). We also quantified the density of comets in either direction, which is the number of comets per unit length of the major dendrite and per unit time of acquisition. There was a significant increase in the plus-end out microtubules in the major dendrite (Supplemental Figure S4D) and not in the minor dendrite (Supplemental Figure S4E) or axon (Supplemental Figure S4F). As the minor dendrite and the axons have plus-end out microtubules, any perturbation in the plus-end out comets is unnoticeable. The comet orientation and density were comparable to wildtype upon expression of *klp-7* cDNA in the wildtype or *klp-7(0)* backgrounds (Figure 4, G–I; Supplemental Figure S4, D–F).

Interestingly, we observed an appearance of the EBP-2::GFP comets in the higher-order branches in the *klp-7* loss of function mutant (Supplemental Figure S4G). In the wild type, EBP-2::GFP comets are present in the primary dendrites and the axon, whereas, in the *klp-7(0)* mutant, these comets also went into secondary branches and sometimes to tertiary branches (Supplemental Figure S4G). This could be due to the ingression of stabilized microtubules in the higher-order branches. Consequentially, it may increase the anterograde traffic of the RAB-3 or SAD-1 vesicles to the higher-order dendrites. Previous results have elucidated that increased stabilization of microtubules in the *klp-7(0)* results in the loss of the minus-end-out microtubule population as visualized by the minus-end reporter PTRN-1 (Puri *et al*., 2021). We checked the presence of the minus end protein PTRN-1::tagRFP in the PVD dendrites to understand whether the minus ends are perturbed due to the loss of the *klp-7* gene. The density of the PTRN-1::tagRFP was comparable between the wildtype and *klp-7(0)* neurons (Supplemental Figure S4, H and I). However, we observed cohesive patches of PTRN-1::tagRFP instead of punctae in the minor dendrite and axonal segments of wild-type neurons. Similar regions were distinctly observable in the major dendrite of *klp-7(0)* neurons (Supplemental Figure S4H). Based on the comet densities and PTRN-1::tagRFP punctae, we concluded that KLP-7 is maintaining the microtubule polarity possibly by forming a dendritic checkpoint that regulates the entry of the plus end-out microtubules into the major dendrite.

Axon Initial Segment (AIS) protein UNC-44 accumulates in the dendrites of *klp-7(0)*

Previous studies have explored the dynamic microtubules in the PVD dendrites and deciphered Ankyrin (UNC-44), CRMP2 (UNC-33), UNC-119, Kinesin-1 (UNC-116), Patronin (PTRN-1), and Ninein (NOCA-2) as the major regulators of microtubule dynamics (Maniar *et al*., 2012; Yan *et al*., 2013; Taylor *et al*., 2015; He *et al*., 2020, 2022). Among these, the Ankyrin family protein, UNC-44 is a major organizer of the AIS that also helps the formation of the parallel bundle of plus-end-out microtubules in the axon through axolemmal immobilization of UNC-33 (CRMP2; He *et al*., 2020). Apart from the diffusion barrier function of the AIS, it acts as a sorting filter for the intracellular cargoes between the somatodendritic and axonal compartments (Burack *et al*., 2000; Al-Bassam *et al*., 2012; Farías *et al*., 2015; Leterrier, 2018; Eichel *et al*., 2022). The reliability of these functions is significantly influenced by various factors, including the structure and dimensions of the cargo, the condition of the microtubules, the interactions between cargo molecules and the cortical cytoskeleton, and the specificity of cargo-motor interactions, among others (Nakata and Hirokawa, 2003; Lewis *et al*., 2009; Kuijpers *et al*., 2016; Balasanyan *et al*., 2017). In *C. elegans*, the loss of AIS components like UNC-44, UNC-119, and UNC-33 resulted in the loss of axon-dendrite compartmentalization (Maniar *et al*., 2012; He *et al*., 2020). It is unclear whether KLP-7 somehow regulates the components of the AIS defining the axon-dendrite compartmentalization in PVD.

To explore the role of KLP-7 in the maintenance of the AIS, we imaged a GFP reporter of UNC-44 in the PVD neurons (He *et al*., 2020). Based on the molecular constitution and function of the mammalian AIS, a homologous structure has been defined in the latero-distal region of the PVD axon (Figure 5A). UNC-44::GFP expressed under its own promoter has ubiquitous expression and is present in all the neurites of PVD neurons (Figure 5B). Mean intensity quantification of UNC-44::GFP in the primary dendrites and AIS showed a remarkable enrichment in the AIS region (Figure 5, B and C). The intensity was highest in the AIS region (cyan arrowheads, Figure 5, B and C). In the *klp-7(0)* mutant, the bona fide AIS (cyan arrowhead) did not show a similar degree of enrichment (Figure 5C). However, in the *klp-7(0)* mutant, the levels of UNC-44::GFP in both the primary dendrites and axon were comparable to those in wild type neurons (Figure 4C). This indicated that differential enrichment of UNC-44 in the AIS as compared with the other neurites requires *klp-7*. Overexpression of the *klp-7* isoform caused a drastic decrease in the UNC-44 enrichment at the AIS with comparable intensities in the dendrites (Figure 5C). In the rescue worms, UNC-44::GFP intensity in the AIS was slightly improved, however, it was not significantly different

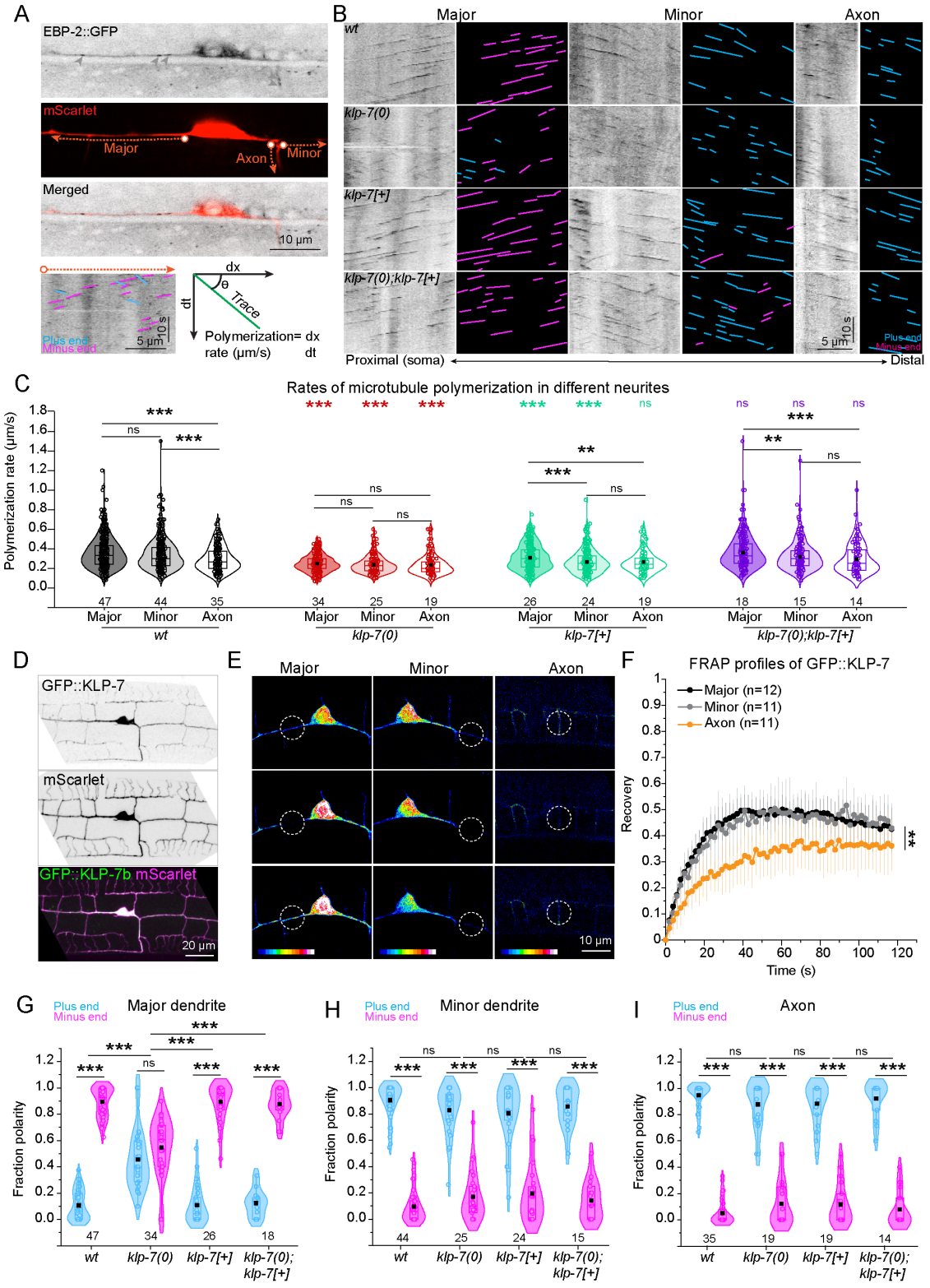

FIGURE 4: Microtubule dynamics and polarity in the PVD dendrites perturbed by loss of *klp-7* function. (A) Representative images of endogenously expressed EBP-2::GFP and PVD neuron expressing mScarlet. Different neurites used for assessing EBP-2::GFP comet dynamics are depicted with orange segmented lines. The origin of the segmented line is marked by a circle, which refers to the proximal region in the kymographs depicted below with plus and minus end out microtubules marked in cyan and magenta, respectively. Traces in the kymographs are measured for the length and time of polymerization, which yield the polymerization rate and angle that provides the orientation of the comets. (B) Kymographs with their respective schematics showing the trajectories of EBP-2::GFP comet in the PVD major dendrite, minor dendrite, and the axonal compartments of the wildtype (*wt*), mutant *klp-7(0)*, *klp-7[+]* overexpression, and *klp-7(0);klp-7[+]* rescue. Schematics show the orientation of the comets in the plus-end-out (cyan)

than the dendritic intensity. This could be due to the formation of bona fide AIS coinciding with or preceding the expression of the *klp-7* transgene under the *ser-2 (prom3)* promoter (Tsalik *et al*., 2003), thus partially rescuing the phenotype.

Interestingly, loss of *klp-7* also results in the formation of ectopic branches that emanate from the cell body (Figure 5B, orange arrowheads). The occurrence of such ectopic branches was quite lower in the wildtype (Supplemental Figure S4A). As compared with the ectopic branches in the wildtype neurons, the *klp-7(0)* neurons showed an enrichment comparable to that of the AIS (Figure 5B). Around 70% of the ectopic branches of the *klp-7(0)* showed AIS-like enrichment as compared with 25% of the wildtype ectopic branches (Supplemental Figure S4A). UNC-44::GFP intensities in the ectopic branches of the PVD neurons of *klp-7(0)* were comparatively higher, than that of wildtype (Figure 5D). In the overexpression and rescue transgenic, the ectopic branches were similar in UNC-44::GFP intensity as those in wildtype (Figure 5D). The formation of AIS coincides with the formation of a polarized array of microtubules by increased stabilization and fasciculation, which are codependent to ensure polarized sorting of the cargoes between axonal and dendritic compartments (Fréal *et al*., 2019). Increased microtubule stabilization in *klp-7* null mutant may enrich UNC-44 in a non-specific manner to PVD dendrites, which causes aberrant sorting of RAB-3, its motor UNC-104, and plus end out microtubules. Recent evidence of ectopic accumulation of TRIM46 in the Kif2a knockout hippocampal neurons (Ruiz-Reig *et al*., 2022) also supports this hypothesis.

The relationship between the proportion of major dendrites with mislocalization of presynaptic cargoes RAB-3/SAD-1, along with the increased ratio of plus-end out microtubules indicated a dependence on KLP-7 depletion for these traits (Figure 6A). Together with this, the formation of ectopic AIS-like dendritic processes in KLP-7 loss of function (Figure 6, B and C) showed how dendrites can attain axon-like identity due to the depletion of KLP-7 function.

DISCUSSION

Our study demonstrates that KLP-7/Kinesin-13 plays a crucial role in regulating the compartmentalization of axons and dendrites in the PVD neurons. Previous studies indicated the importance of Kinesin-13 in establishing dendritic identity (Homma *et al*., 2018). In this study, we shared a mechanistic angle on how the activity of KLP-7 is related to the differential level of microtubule dynamics in dendrite versus axon. Increased microtubule instability driven by KLP-7 is key to preventing the accumulation of AIS components in the dendrites, delimiting the entry of axonal proteins into dendrites (Figure 6). This provides new insight into how microtubule instability and AIS element Ankyrin/UNC-44 are antagonistically related to control neuronal polarity (Figure 6).

KLP-7/Kinesin-13 dependent microtubule organization regulates the axon dendrite compartmentalization

Neuronal polarization commences with axon specification (Dotti *et al*., 1988; Higgs and Das, 2022) determined by microtubule stabilization and bundling (Witte *et al*., 2008; Van Beuningen *et al*., 2015). The stability of the microtubules imparts strength to the growing axon, provides a platform for other cytoskeletal interactions, promotes selective trafficking of molecules, and generates force for changes in morphology during growth (Hawkins *et al*., 2010; Kapitein and Hoogenraad, 2011). It is unclear how microtubule catastrophe factors, which also contribute to the dynamic instability of microtubules participate in neuronal polarization.

Loss of Kinesin-13/KIF2/KLP-7 causes an aberrant arborization of neurons with defects in axon-dendrite compartmentalization and premature degeneration (Homma *et al*., 2018; Puri *et al*., 2021; Ruiz-Reig *et al*., 2022). Conditional KIF2 knockout animals also showed behavioral defects like epilepsy (Homma *et al*., 2018; Partoens *et al*., 2021). Mechanistic insight into these phenotypes due to the loss of Kinesin 13 was lacking. We found that microtubule stabilization in the loss of function of KLP-7 (Kinesin-13) could lead to the formation of multiple axon-like neurites during development, similar to that observed upon Taxol treatment (Witte *et al*., 2008). We showed other microtubule depolymerizers like EFA-6 did not affect the axon-dendrite compartmentalization. We could significantly suppress the defect of the *klp-7* null mutant by Colchicine treatment and fully rescue by cell-autonomous expression of *klp-7* transgene, indicating additional roles of KLP-7 besides microtubule stabilization in preserving the axon-dendrite compartmentalization.

KLP-7 is a microtubule depolymerizing enzyme, and under the Wnt signaling, its differential activity in the PLM neurites regulates its microtubule organization (Desai *et al*., 1999; Puri *et al*., 2021). but it was unclear how KLP-7 organizes the microtubules in the PVD neurons. We showed that loss of *klp-7* resulted in decreased polymerization and a mixed orientation of microtubules in the major dendrite, which typically has minus end-out microtubule polarity. In other neurites with plus end out polarity, that is, minor and axon, the polymerization dynamics were affected, but the polarity of the microtubules was unchanged by *klp-7* deletion. In the *klp-7* null mutant, apart from an increase in the plus-end out EBP-2::GFP comets, we observed a concomitant decrease in the minus-end out microtubules, which rules out the possibility of specific depolymerization of plus-end out microtubules by KLP-7 in the major dendrite. Furthermore, overexpression of *klp-7* did not perturb the polarity of microtubules in the major dendrite. It could be an effect of global disruption of intraneuronal trafficking of cargoes, including axonal cargoes and microtubules.

and minus-end-out (magenta) directions. (C) Rates of polymerization were quantified as the covered distance divided by the duration of the EBP-2::GFP comets in the PVD major dendrite, minor dendrite, and the axon of the wildtype (*wt*), mutant *klp-7(0)*, *klp-7[+]* overexpression, and *klp-7(0);klp-7[+]* rescue. Comparison of means was done using ANOVA and Bonferroni Test. $p < 0.001$***. Number of animals assessed (n) is mentioned along the X-axis. (D) Representative image showing the major, minor, and axonal compartments to assess the distribution of GFP::KLP-7 (5 ng extrachromosomal array) in the PVD neuron. (E and F) Representative images (E) of FRAP assay of GFP::KLP-7 in various compartments quantified as recovery profiles (F). Number of animals assessed (n) is mentioned in the legend. Comparison of maximum recovery was done using ANOVA and Bonferroni Test. $p < 0.01$**. Data points represent Mean±S.D. (G–I) Relative orientation of the microtubules is represented as a fraction polarity of EBP-2::GFP comets in the plus-end-out (cyan) and minus-end-out directions (magenta) in the PVD major dendrite (G), minor dendrite (H), and the axon (I) of the wildtype (*wt*), mutant *klp-7(0)*, *klp-7[+]* overexpression, and *klp-7(0);klp-7[+]* rescue. Comparison of means was done using ANOVA and Bonferroni Test. $p < 0.001$***, ns (not significant). Number of animals assessed (n) is mentioned along the X-axis.

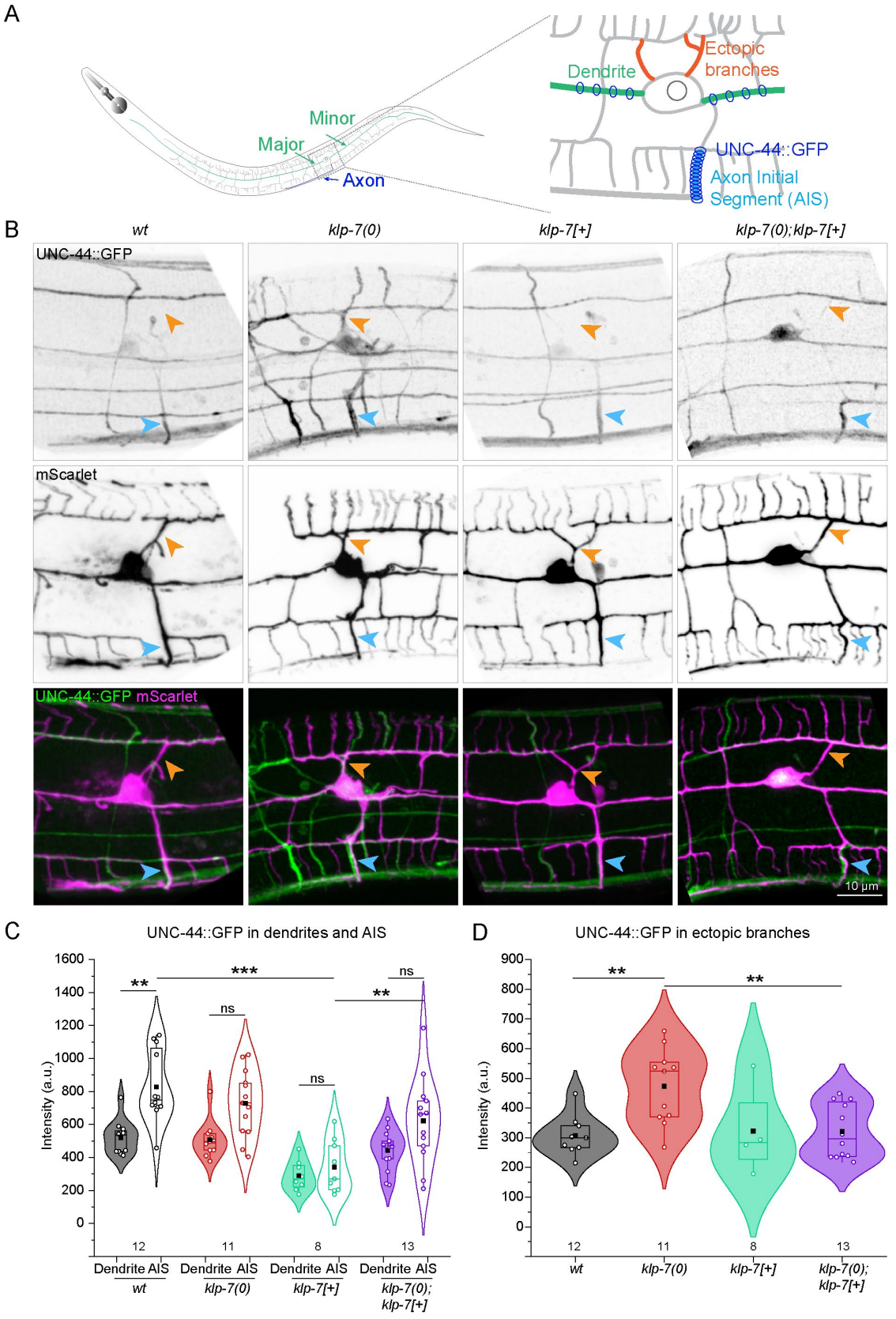

FIGURE 5: Specific enrichment of AIS protein, UNC-44 is dependent on *klp-7* function. (A) Schematic showing the dendrites (major and minor), ectopic branches, and AIS compartments to assess the distribution of UNC-44::GFP in a typical PVD neuron magnified in the middle panel. (B) Representative images of the PVD neuron in wildtype (*wt*), mutant *klp-7(0)*, *klp-7[+]* overexpression, and *klp-7(0);klp-7[+]* rescue expressing mScarlet and single copy insertion of UNC-44::GFP under its endogenous promoter. Yellow and cyan arrowheads depict the ectopic branches and AIS of the PVD

KLP-7 negatively regulates the formation and integrity of the AIS-like sorting filters in the PVD neurites

Previous studies have explored neuronal polarity in the PVD neurons and have found the role of UNC-44, UNC-33, UNC-119, TIAM-1, PTRN-1 and NOCA-2 (Maniar *et al.*, 2012; He *et al.*, 2020, 2022; Lin *et al.*, 2022). In the loss of function mutants of these genes, besides the mislocalization of axonal cargoes in the dendrites, microtubule polarity in the neurites was also perturbed (Maniar *et al.*, 2012; He *et al.*, 2020, 2022; Lin *et al.*, 2022). Additional mechanisms like mislocalization of UNC-104 to dendrites, defects in Kinesin-1 mediated microtubule sliding, loss of cytoskeletal interactions, and possible defects in microtubule nucleation were also associated with these mutants (Maniar *et al.*, 2012; He *et al.*, 2020, 2022; Lin *et al.*, 2022). It was unclear how microtubule depolymerizing enzymes such as KLP-7 coordinate with these molecules to regulate the microtubule organization and neuronal polarity.

An aberrant transport of axonal proteins in the major dendrite in the *klp-7(0)* could be due to the ectopic formation of AIS-like sorting filter in these dendrites. The AIS serves two critical functions in neurons: 1.) Acting as a diffusion filter to regulate the movement of cytoplasmic and membrane proteins (Winckler *et al.*, 1999; Nakada *et al.*, 2003; Albrecht *et al.*, 2016; Eichel *et al.*, 2022), 2.) Sorting intracellular cargo between the axonal and somatodendritic compartments both before and within the AIS (Burack *et al.*, 2000; Al-Bassam *et al.*, 2012; Farías *et al.*, 2015; Leterrier, 2018; Eichel *et al.*, 2022). The effectiveness of these functions relies heavily on factors such as the cargo structure and size, the condition of microtubules, interactions between cargo molecules and the cortical cytoskeleton, and the specificity of cargo-motor interactions (Nakata and Hirokawa, 2003; Lewis *et al.*, 2009; Kuijpers *et al.*, 2016; Balasanyan *et al.*, 2017). Previous studies in the *C. elegans* system have demonstrated that UNC-44 is essential for the function of the AIS, which restricts axonal cargoes such as RAB-3 and somatodendritic cargoes such as DMA-1 to their respective compartments (Maniar *et al.*, 2012; He *et al.*, 2020; Eichel *et al.*, 2022). Loss of UNC-44 also perturbs the microtubule orientation in the dendrites towards an increase in the plus end out microtubules, which may support the movement of anterograde cargoes (Maniar *et al.*, 2012; He *et al.*, 2020). These results indicate that the axonal microtubules, motors, and cargoes prefer the neurites where UNC-44 is likely to be in a membrane-anchored complex with UNC-119 and UNC-33L (large isoform; He *et al.*, 2020).

Although the AIS protein Ankyrin/UNC-44 was ubiquitously localized to all neurites of PVD, normalized intensity of this protein in the wildtype PVD neurons showed a marked enrichment in the bona fide AIS defined as per the molecular constitution akin to mammalian AIS (Maniar *et al.*, 2012; He *et al.*, 2020). Loss of *klp-7* affected the selective enrichment of UNC-44::GFP in the AIS with additional enrichment of UNC-44::GFP in dendritic branches. This was conspicuous in the ectopic branches emanating from the cell bodies of PVD neurons. Though this anatomical feature was rare in wildtype animals, these branches showed an excess of UNC-44::GFP in the deletion mutant of *klp-7*. This result corroborated previous observations of mosaic arbors in *Drosophila* class IV ddaC neurons upon Patronin RNAi with ectopic accumulation of AIS components and hippocampal neurons of Kif2A conditional knockout rodents with ectopic TRIM46 enrichment (Ruiz-Reig *et al.*, 2022; Thyagarajan *et al.*, 2022).

Formation of AIS in the axon correlates well with the decreased dynamics of microtubule polymerization and GFP::KLP-7. In developing anterior PVD dendrite, the UNC-44/UNC-33 complex is excluded from the distal MTOC where dynamic microtubules are prevalent (Liang *et al.*, 2024). In our study, in the absence of catastrophe factor KLP-7, microtubules are relatively stable and the complex of UNC-44/UNC-119/UNC-33/nondepolymerizing microtubules is probably stabilized and forms a sorting structure akin to AIS. Our results of *klp-7* overexpression, which perturbed the bonafide localization of UNC-44::GFP at the AIS strengthened this hypothesis. AIS-type accumulations of UNC-44 in the dendrites may serve as conduits for axonal traffic. Due to loss of *klp-7*, axon-specific motor UNC-104 was significantly increased in the dendrites indicating most of the axonal traffic to be also present in the dendrites. KLP-7 activity in the dendrites regulates the microtubule polymerization and dynamics, which further prevent the formation and integrity of the AIS-like sorting filters thereby restricting the traffic of axonal microtubules, motors, and cargoes. The conditions that allow axonal traffic into any neurite appear to be the presence of AIS components, and stable and plus-end out microtubules which are fulfilled in the *klp-7(0)* dendrites.

Overall, our study sheds light on the intricate mechanisms underlying the regulation of axon-dendrite compartmentalization through KLP-7-mediated microtubule regulation and AIS formation and integrity (Figure 6, B and C).

MATERIALS AND METHODS

Request a protocol through *Bio-protocol*.

C. elegans culturing, constructs, and transgenesis

The worms were cultured on the Nematode Growth Medium (NGM) seeded with OP50 bacteria at 20°C. Mutants and transgenics were crossed, and homozygosity of mutant and transgene alleles was confirmed by genotyping and phenotyping. The mutant and transgenes are mentioned in Supplemental Table S1. The allele *kyIs445 [pdes-2::mCherry::RAB-3 (0.5 ng/µl); pdes-2::SAD-1::GFP (2 ng/µl); podr-1::DsRed (30 ng/µl)]* is a gift from Cory Bargmann lab, *ebp-2*(*wow47* [*ebp-2::gfp::3xflag*]) is a gift from Feldman lab and. To generate shrEx483, young adult worms were microinjected with 5 ng/µl of *pser2prom3::gfp::klp-7b*, 10 ng/µl of *pser2prom3::mScarlet*, and 50 ng/µl of *pttx-3::rfp*. The construct of *pser2prom3::gfp::klp-7b* was generated using the InFusion cloning. Similarly, shrEx490 was generated by microinjecting 15 ng/µl of *pser2prom3:: klp-7b*, 10 ng/µl of *pser2prom3::mScarlet*, and 2 ng/µl of *pmyo-2::mCherry*.

Sample preparation

Neuronal polarity was assayed in L4 staged worms for both control and mutant conditions. The worms were harvested after a definite

neuron. (C) Mean intensities of UNC-44::GFP in the dendrites (major and minor) and AIS of PVD neurons of wildtype (*wt*), mutant *klp-7(0), klp-7[+]* overexpression, and *klp-7(0);klp-7[+]* rescue. Comparison of means was done using ANOVA and Bonferroni Test. $p < 0.01$**, 0.001***, ns (not significant). Number of animals assessed (n) is mentioned along the X-axis. (D) Ectopic branches emanating from the cell bodies of wildtype (*wt*), mutant *klp-7(0), klp-7[+]* overexpression, and *klp-7(0);klp-7[+]* rescue neurons were assessed for their enrichment and quantified as the mean intensity of UNC-44::GFP. Comparison of means was done using ANOVA and Bonferroni Test. $p < 0.01$**, 0.001***, ns (not significant). Number of animals assessed (n) is mentioned along the X-axis.

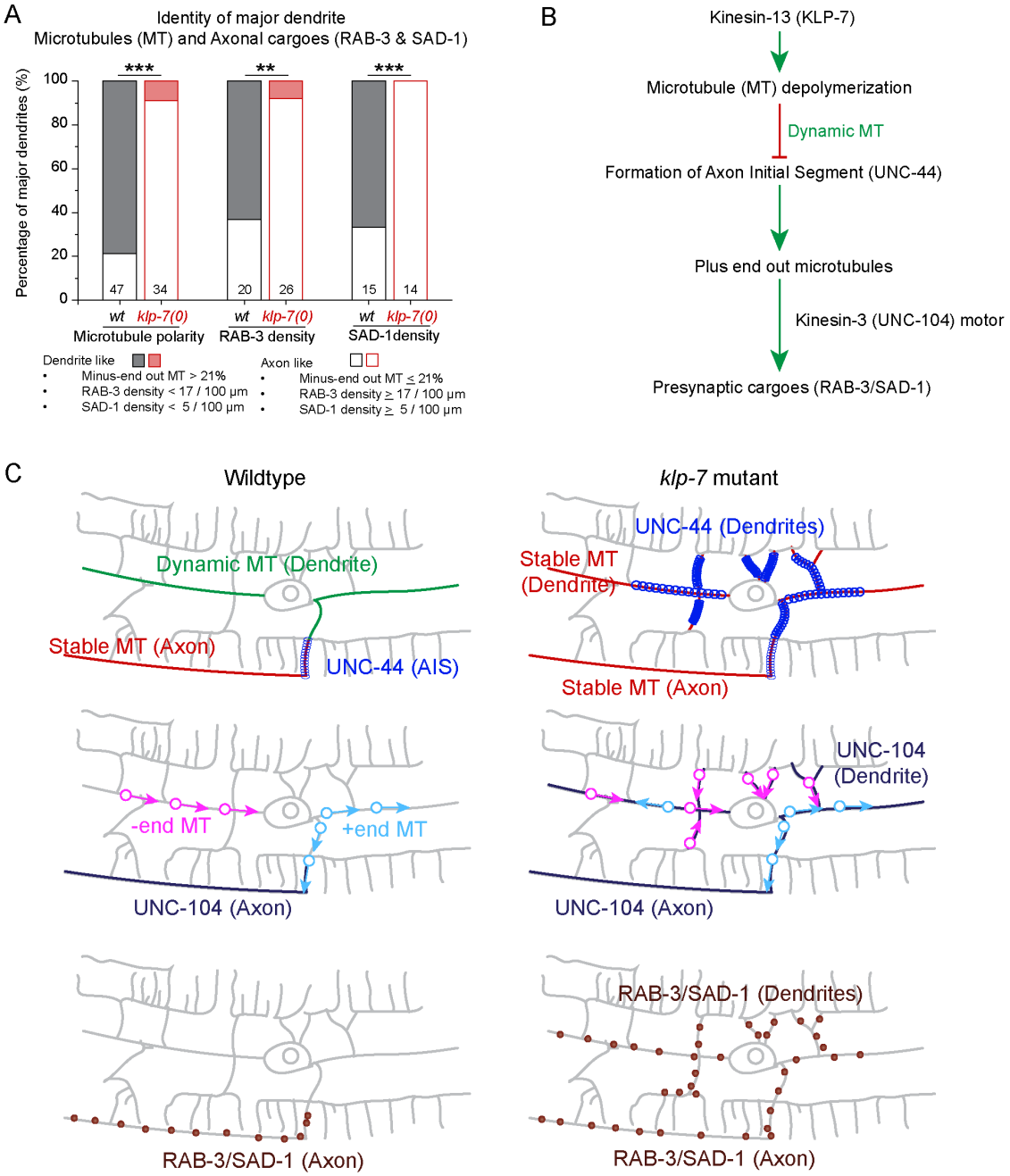

FIGURE 6: KLP-7 mediated axonal checkpoint determining axonal sorting of cargoes and microtubules. (A) Proportion of major dendrites with characteristic features of dendrite and axon differentiated based on microtubule polarity, RAB-3, and SAD-1 densities in the wildtype (wt) and *klp-7(0)* mutant represented as a stacked bar graph. The criteria are defined by the mean value of each feature in the wildtype major dendrite as mentioned in the legend. The filled and open areas in each stacked bar represent the proportions with dendrite and axon-like characteristics, respectively. Comparison between *wt* and *klp-7(0)* was done using Fisher's exact test. $p < 0.01$**, 0.001***. Number of animals assessed (n) is mentioned along the X-axis. (B) Microtubule depolymerization activity of Kinesin-13 (KLP-7) maintains differential microtubule dynamics in the dendrites and axons. The presence of dynamic microtubules due to this activity prevents the enrichment of Ankyrin (UNC-44) in dendrites of wild-type neurons. Specific enrichment of UNC-44 in the AIS ensures trafficking of plus end out microtubules, axonal motor (UNC-104), and presynaptic cargoes into the axon only. (C) Graphical representation of wildtype and *klp-7(0)* PVD neurons. The absence of microtubule depolymerization in the *klp-7(0)*, decreases the microtubule dynamics in dendrites as well as axons leading to ectopic enrichment of UNC-44. Enrichment of UNC-44 in the AIS of wildtype or dendrites of *klp-7(0)* directs the axonal traffic of plus end microtubules and axonal motor, UNC-104, and presynaptic cargoes (RAB-3 and SAD-1) in these compartments. Accumulation of AIS component UNC-44, plus end-out microtubules, axonal motor UNC-104, and presynaptic cargoes RAB-3/SAD-1 in processes other than axon attributes axon-like identity to such processes.

period and, are mounted on 7.5% agarose pads using a cocktail of 0.1% Tricaine and 10 mM Tetramisole.

For imaging of microtubule-associated End Binding Protein (EBP) comets, the worms were mounted on 10% agarose pads in a mounting medium of 0.1µm polystyrene beads. A maximum of five to seven worms were mounted simultaneously for imaging. For FRAP assays, the mounting was done in a mixture of 0.1% Tricaine and 10 mM Tetramisole as described before.

Worms were grown on Colchicine (1 mM) containing NGM plates because hatching for the pharmacological perturbation of the microtubules.

Microscopy

Worms were imaged on the Nikon A1R confocal using 60X/1.4NA oil objective at a voxel scale of 0.414 µm x 0.414 µm x 1.0 µm. A large area scanning was enabled to image the whole worm. To image multiple reporters sequential channel imaging was used. For some ubiquitously expressed reporters like UNC-104::GFP, and UNC-44::GFP, the imaging was carried out at a voxel scale of 0.09 µm x 0.09 µm x 0.125 µm using 60X/1.4NA oil objective.

Live imaging of EBP comets was carried out on the Zeiss Observer.Z1 inverted microscope equipped with Yokogawa CSU-X1 spinning disk unit and Photometrics Evolve camera. Imaging was carried out on a 100X/1.4NA oil objective at a temporal resolution of one frame per second for 2 min.

mCherry::RAB-3 particles were observed using Zeiss Observer. Z1 inverted microscope equipped with Yokogawa CSU-X1 spinning disk unit and Photometrics Evolve camera. Imaging was done on a 100X/1.4NA oil objective at a temporal resolution of 1.4 frames per second for 2 min.

FRAP assays were carried out on the Nikon A1R confocal using 60X/1.4NA oil objective at a voxel scale of 0.09 µm × 0.09 µm × 0.2 µm. A circular region of 5-µm diameter was chosen for the photobleaching, and the entire acquisition was carried out at a frame rate of one frame per second. Before photobleaching, five frames were collected, photobleaching was carried out for 5 s, and post photobleaching acquisition was carried out for a duration of 2 min.

Analysis

Neuronal polarity has been assayed by the percentage of dendrites with mCherry::RAB-3, density of mCherry::RAB-3 punctae, and population of worms with dendritic SAD-1::GFP in the primary dendrites. The percentage of dendrites and population distribution has been assessed manually by locating punctae over a particular threshold intensity. This threshold has been set by the intensity of the mCherry::RAB-3 punctae present in the axon (ventral nerve cord) in the wildtype neurons. The density and mean intensities of mCherry::RAB-3 or SAD-1::GFP punctae have been assessed by the line profile of intensities in the primary dendrites and peak finding tool using the BAR plugin in ImageJ (Fiji). The density of the punctae was calculated by the number of punctae divided by the length of the neurite while the peak intensities averaged for all punctae in the assessed neurite yield the mean intensity. Relative density and mean intensity were obtained by normalizing dendritic values with axonal values. PTRN-1::tagRFP punctae were also analyzed for their density in the primary dendrites using the line profile and peak finding tool using the BAR plugin in ImageJ. For quantification of neuroprevalent reporters like UNC-104::GFP and UNC-44::GFP in the PVD neurites, we used the constitutive reporter mScarlet for tracing neurites using the SNT plugin in ImageJ (Fiji). From the linescan profile of each neurite for the reporters (UNC-104::GFP or UNC-44::GFP), intensities and lengths of the neurite were obtained. The total of the intensities was divided by the length of the neurite to obtain the intensity per unit length of the neurite.

Timelapse acquisitions of EBP-2::GFP comets were analyzed in ImageJ by extracting kymographs from different neurites of PVD neurons. The traces in the kymographs were assessed using the line tool to obtain the angle, length, and duration. Slopes of the traces obtained from the angles were used for the orientation of the comets. The length of the traces was divided by their duration to obtain the rates of polymerization.

The images and videos were quantified using ImageJ. All the images were background-corrected and normalized to the maximum. Intensities obtained from the FRAP region were normalized to prebleach and postbleach intensities and plotted against time. The FRAP curves were fitted to the following single exponential equation using the Levenberg-Marquardt iteration algorithm in Origin:

$$I_t(t) = I_{max}(I - e^{-\tau * t})$$

The maximum recovery amplitude (I_{max}) and the half-time ($t_{1/2}$ = ln 0.5/–τ) parameters were obtained from the fit.

Intensities in a given neurite were quantified from a line ROI spanning across multiple optical sections and normalized with a constitutive marker.

Data representation and statistics

Quants obtained from ImageJ were fed into Excel and Origin to get statistically relevant data. The data has been plotted as violin and box-whisker plots with individual values. The mean value is represented by black squares within the plots. Significance values of $p <$ 0.05*, 0.01**, and 0.001*** are marked within the plots between the compared datasets. Relevant nonsignificant comparisons have been marked by "ns." The number of organisms tested is mentioned in the respective plots. Each experimental dataset has been obtained from a minimum of $N = 3$ experiments carried out across multiple generations of the worm strain or condition. Parametric data were compared using ANOVA and Bonferroni test. Nonparametric datasets were compared using Fisher's exact test and are mentioned in the figure legends.

ACKNOWLEDGMENTS

We thank Dr. Jessica Feldman for the CRISPR allele of EBP-2::GFP, Dr. Cornelia Bargmann for the RAB-3 and SAD-1 reporter strain, Dr. Sandhya P. Koushika for the UNC-104 reporter strain and Caenorhabditis Genetics Center (CGC) for mutant and transgenic strains. CGC is supported by the National Institutes of Health Office of Research Infrastructure Programs (P40 OD010440). This work is supported by the NBRC core fund from the Department of Biotechnology, and DBT/Wellcome Trust India Alliance (Grant # IA/E/13/1/504331 to S.D., Grant # IA/I/13/1/500874 to A.G.-R.).

REFERENCES

Al-Bassam S, Xu M, Wandless TJ, Arnold DB (2012). Differential Trafficking of Transport Vesicles Contributes to the Localization of Dendritic Proteins. Cell Rep 2, 89–100.

Albeg A, Smith CJ, Chatzigeorgiou M, Feitelson DG, Hall DH, Schafer WR, Miller DM, Treinin M (2011). C. elegans multi-dendritic sensory neurons: Morphology and function. Mol Cell Neurosci 46, 308–317.

Albrecht D, Winterflood CM, Sadeghi M, Tschager T, Noé F, Ewers H (2016). Nanoscopic compartmentalization of membrane protein motion at the axon initial segment. J Cell Biol 215, 37–46.

Arimura N, Menager C, Fukata Y, Kaibuchi K (2004). Role of CRMP-2 in neuronal polarity. J Neurobiol 58, 34–47.

Baas PW, Slaughter T, Brown A, Black MM (1991). Microtubule dynamics in axons and dendrites. J Neurosci Res 30, 134–153.

Baas PW, Rao AN, Matamoros AJ, Leo L (2016). Stability properties of neuronal microtubules. Cytoskeleton 73, 442–460.
Balasanyan V, Watanabe K, Dempsey WP, Lewis TL, Trinh LA, Arnold DB (2017). Structure and function of an actin-based filter in the proximal axon. Cell Rep 21, 2696–2705.
Barnes AP, Polleux F (2009). Establishment of Axon-Dendrite polarity in developing neurons. Annu Rev Neurosci 32, 347–381.
Bounoutas A, Kratz J, Emtage L, Ma C, Nguyen KC, Chalfie M (2011). Microtubule depolymerization in Caenorhabditis elegans touch receptor neurons reduces gene expression through a p38 MAPK pathway. Proc Natl Acad Sci USA 108, 3982–3987.
Brar HK, Dey S, Singh P, Pande D, Ghosh-Roy A (2024). Functional recovery associated with dendrite regeneration in PVD neuron of C. elegans. ENeuro 11, ENEURO.0292-23.2024.
Burack MA, Silverman MA, Banker G (2000). The role of selective transport in neuronal protein sorting. Neuron 26, 465–472.
Cavallin M, Bijlsma EK, El Morjani A, Moutton S, Peeters EAJ, Maillard C, Pedespan JM, Guerrot AM, Drouin-Garaud V, Coubes C, *et al.* (2017). Recurrent KIF2A mutations are responsible for classic lissencephaly. Neurogenetics 18, 73–79.
Chalfie M, Thomson JN (1982). Structural and functional diversity in the neuronal microtubules of Caenorhabditis elegans. J Cell Biol 93, 15–23.
Chatzigeorgiou M, Yoo S, Watson JD, Lee WH, Spencer WC, Kindt KS, Hwang SW, Miller DM 3rd, Treinin M, Driscoll M, *et al.* (2010). Specific roles for DEG/ENaC and TRP channels in touch and thermosensation in C. elegans nociceptors. Nat Neurosci 13, 861–868.
Chen L, Chuang M, Koorman T, Boxem M, Jin Y, Chisholm AD (2015). Axon injury triggers EFA-6 mediated destabilization of axonal microtubules via TACC and doublecortin like kinase. eLife 4, e08695.
Cong D, Ren J, Zhou Y, Wang S, Liang J, Ding M, Feng W (2021). Motor domain-mediated autoinhibition dictates axonal transport by the kinesin UNC-104/KIF1A. PLOS Genet 17, e1009940.
Costain G, Cordeiro D, Matviychuk D, Mercimek-Andrews S (2019). Clinical application of targeted next-generation sequencing panels and whole exome sequencing in childhood epilepsy. Neuroscience 418, 291–310.
Crump JG, Zhen M, Jin Y, Bargmann CI (2001). The SAD-1 kinase regulates presynaptic vesicle clustering and axon termination. Neuron 29, 115–129.
Dehmelt L, Nalbant P, Steffen W, Halpain S (2006). A microtubule-based, dynein-dependent force induces local cell protrusions: Implications for neurite initiation. Brain Cell Biol 35, 39–56.
Desai A, Verma S, Mitchison TJ, Walczak CE (1999). Kin I kinesins are microtubule-destabilizing enzymes. Cell 96, 69–78.
Dotti CG, Sullivan CA, Banker GA (1988). The establishment of polarity by hippocampal neurons in culture. J Neurosci 8, 1454–1468.
Eichel K, Uenaka T, Belapurkar V, Lu R, Cheng S, Pak JS, Taylor CA, Südhof TC, Malenka R, Wernig M, *et al.* (2022). Endocytosis in the axon initial segment maintains neuronal polarity. Nat 609, 128–135.
Farías GG, Guardia CM, Britt DJ, Guo X, Bonifacino JS (2015). Sorting of Dendritic and Axonal Vesicles at the Pre-axonal Exclusion Zone. Cell Rep 13, 1221–1232.
De Forges H, Bouissou A, Perez F (2012). Interplay between microtubule dynamics and intracellular organization. Int J Biochem Cell Biol 44, 266–274.
Franco M, Peters PJ, Boretto J, Van Donselaar E, Neri A, D'Souza-Schorey C, Chavrier P (1999). EFA6, a sec7 domain-containing exchange factor for ARF6, coordinates membrane recycling and actin cytoskeleton organization. EMBO J 18, 1480–1491.
Fréal A, Rai D, Tas RP, Pan X, Katrukha EA, van de Willige D, Stucchi R, Aher A, Yang C, Altelaar AFM, *et al.* (2019). Feedback-driven assembly of the axon initial segment. Neuron 104, 305–321.e8.
Ghosh-Roy A, Goncharov A, Jin Y, Chisholm AD (2012). Kinesin-13 and tubulin posttranslational modifications regulate microtubule growth in axon regeneration. Dev Cell 23, 716–728.
Gudimchuk NB, McIntosh JR (2021). Regulation of microtubule dynamics, mechanics and function through the growing tip. Nat Rev Mol Cell Biol 2021 2212 22, 777–795.
Hall DH, Hedgecock EM (1991). Kinesin-related gene unc-104 is required for axonal transport of synaptic vesicles in C. elegans. Cell 65, 837–847.
Harterink M, Edwards SL, de Haan B, Yau KW, van den Heuvel S, Kapitein LC, Miller KG, Hoogenraad CC (2018). Local microtubule organization promotes cargo transport in C. elegans dendrites. J Cell Sci 131, jcs.223107.
Hawkins T, Mirigian M, Selcuk Yasar M, Ross JL (2010). Mechanics of microtubules. J Biomech 43, 23–30.
He L, Kooistra R, Das R, Oudejans E, van Leen E, Ziegler J, Portegies S, de Haan B, Altena A van R, Stucchi R, *et al.* (2020). Cortical anchoring of the microtubule cytoskeleton is essential for neuron polarity. eLife 9, e55111.
He L, van Beem L, Snel B, Hoogenraad CC, Harterink M (2022). PTRN-1 (CAMSAP) and NOCA-2 (NINEIN) are required for microtubule polarity in Caenorhabditis elegans dendrites. PLOS Biol 20, e3001855.
Helenius J, Brouhard G, Kalaidzidis Y, Diez S, Howard J (2006). The depolymerizing kinesin MCAK uses lattice diffusion to rapidly target microtubule ends. Nat 2006 4417089 441, 115–119.
Higgs VE, Das RM (2022). Establishing neuronal polarity: microtubule regulation during neurite initiation. Oxford Open Neurosci 1, 1–19.
Hirokawa N, Niwa S, Tanaka Y (2010). Molecular motors in neurons: transport mechanisms and roles in brain function, development, and disease. Neuron 68, 610–638.
Homma N, Takei Y, Tanaka Y, Nakata T, Terada S, Kikkawa M, Noda Y, Hirokawa N (2003). Kinesin superfamily protein 2A (KIF2A) functions in suppression of collateral branch extension. Cell 114, 229–239.
Homma N, Zhou R, Naseer MI, Chaudhary AG, Al-Qahtani MH, Hirokawa N (2018). KIF2A regulates the development of dentate granule cells and postnatal hippocampal wiring. eLife 7, e30935.
Horio T, Murata T, Murata T (2014). The role of dynamic instability in microtubule organization. Front Plant Sci 5, 1–11.
Kapitein LC, Hoogenraad CC (2011). Which way to go? Cytoskeletal organization and polarized transport in neurons. Mol Cell Neurosci 46, 9–20.
Kapitein LC, Hoogenraad CC (2015). Building the Neuronal Microtubule Cytoskeleton. Neuron 87, 492–506.
Kapitein LC, Schlager MA, Kuijpers M, Wulf PS, van Spronsen M, MacKintosh FC, Hoogenraad CC (2010). Mixed microtubules steer dynein-driven cargo transport into dendrites. Curr Biol 20, 290–299.
Karabay A, Yu W, Solowska JM, Baird DH, Baas PW (2004). Axonal growth is sensitive to the levels of katanin, a protein that severs microtubules. J Neurosci 24, 5778–5788.
Kelliher MT, Saunders HA, Wildonger J (2019). Microtubule control of functional architecture in neurons. Curr Opin Neurobiol 57, 39–45.
Kirszenblat L, Neumann B, Coakley S, Hilliard MA (2013). A dominant mutation in mec-7/βtubulin affects axon development and regeneration in Caenorhabditis elegans neurons. Mol Biol Cell 24, 285–296.
Kuijpers M, van de Willige D, Freal A, Chazeau A, Franker MA, Hofenk J, Rodrigues RJC, Kapitein LC, Akhmanova A, Jaarsma D, *et al.* (2016). Dynein regulator NDEL1 controls polarized cargo transport at the axon initial segment. Neuron 89, 461–471.
Kuijpers M, Hoogenraad CC (2011). Centrosomes, microtubules and neuronal development. Mol Cell Neurosci 48, 349–358.
Kumar J, Choudhary BC, Metpally R, Zheng Q, Nonet ML, Ramanathan S, Klopfenstein DR, Koushika SP (2010). The Caenorhabditis elegans Kinesin-3 Motor UNC-104/KIF1A is degraded upon loss of specific binding to cargo. PLOS Genet 6, e1001200.
Leterrier C (2018). The Axon initial segment: an updated viewpoint. J Neurosci 38, 2135–2145.
Lewis TL, Mao T, Svoboda K, Arnold DB (2009). Myosin-dependent targeting of transmembrane proteins to neuronal dendrites. Nat Neurosci 2009 125 12, 568–576.
Li LB, Lei H, Arey RN, Li P, Liu J, Murphy CT, Xu XZS, Shen K (2016). The neuronal kinesin UNC-104/KIF1A is a key regulator of synaptic aging and insulin signaling-regulated memory. Curr Biol 26, 605–615.
Li W, Miki T, Watanabe T, Kakeno M, Sugiyama I, Kaibuchi K, Goshima G (2011). EB1 promotes microtubule dynamics by recruiting Sentin in Drosophila cells. J Cell Biol 193, 973–983.
Liang X, Agulto R, Eichel K, Taylor CA, Paat VA, Deng H, Ori-McKenney K, Shen K (2024). CRMP/UNC-33 maintains neuronal microtubule arrays by promoting individual microtubule rescue. BioRxiv, 1–41.
Lin CH, Chen YC, Chan SP, Ou CY (2022). TIAM-1 differentially regulates dendritic and axonal microtubule organization in patterning neuronal development through its multiple domains. PLoS Genet 18, e1010454.
Lockhead D, Schwarz EM, O'hagan R, Bellotti S, Krieg M, Barr MM, Dunn AR, Sternberg PW, Goodman MB (2016). The tubulin repertoire of Caenorhabditis elegans sensory neurons and its context-dependent role in process outgrowth. Mol Biol Cell 27, 3717.
Maeder CI, Shen K, Hoogenraad CC (2014). Axon and dendritic trafficking. Curr Opin Neurobiol 27, 165–170.
Maniar TA, Kaplan M, Wang GJ, Shen K, Wei L, Shaw JE, Koushika SP, Bargmann CI (2012). UNC-33 (CRMP) and ankyrin organize microtubules and localize kinesin to polarize axon-dendrite sorting. Nat Neurosci 15, 48–56.
Marín O, Valiente M, Ge X, Tsai LH (2010). Guiding neuronal cell migrations. Cold Spring Harb Perspect Biol 2, a001834.

Moriwaki T, Goshima G (2016). Five factors can reconstitute all three phases of microtubule polymerization dynamics. J Cell Biol 215, 357–368.
Nakada C, Ritchie K, Oba Y, Nakamura M, Hotta Y, Iino R, Kasai RS, Yamaguchi K, Fujiwara T, Kusumi A (2003). Accumulation of anchored proteins forms membrane diffusion barriers during neuronal polarization. Nat Cell Biol 2003 57 5, 626–632.
Nakata T, Hirokawa N (2003). Microtubules provide directional cues for polarized axonal transport through interaction with kinesin motor head. J Cell Biol 162, 1045–1055.
O'Rourke SM, Christensen SN, Bowerman B (2010). C. elegans EFA-6 Limits Microtubule Growth at the Cell Cortex. Nat Cell Biol 12, 1235.
Ogawa T, Hirokawa N (2015). Microtubule destabilizer KIF2A undergoes distinct site-specific phosphorylation cascades that differentially affect neuronal morphogenesis. Cell Rep 12, 1774–1788.
Ogawa T, Saijo S, Shimizu N, Jiang X, Hirokawa N (2017). Mechanism of catalytic microtubule depolymerization via KIF2-Tubulin transitional conformation. Cell Rep 20, 2626–2638.
Partoens M, De Meulemeester AS, Giong HK, Pham DH, Lee JS, De Witte PA, Siekierska A (2021). Modeling neurodevelopmental disorders and Epilepsy caused by loss of function of kif2a in zebrafish. ENeuro 8, 1–17.
Poirier K, Lebrun N, Broix L, Tian G, Saillour Y, Boscheron C, Parrini E, Valence S, Pierre BS, Oger M, *et al*. (2013). Mutations in TUBG1, DYNC1H1, KIF5C and KIF2A cause malformations of cortical development and microcephaly. Nat Genet 45, 639–647.
Polleux F, Snider W (2010). Initiating and growing an axon. Cold Spring Harb Perspect Biol 2, a001925.
Puri D, Ponniah K, Biswas K, Basu A, Dey S, Lundquist EA, Ghosh-Roy A (2021). Wnt signaling establishes the microtubule polarity in neurons through regulation of Kinesin-13. J Cell Biol 220, e202005080.
Qiang L, Yu W, Andreadis A, Luo M, Baas PW (2006). Tau protects microtubules in the axon from severing by katanin. J Neurosci 26, 3120–3129.
Qu Y, Hahn I, Lees M, Parkin J, Voelzmann A, Dorey K, Rathbone A, Friel CT, Allan VJ, Okenve-Ramos P, *et al*. (2019). Efa6 protects axons and regulates their growth and branching by inhibiting microtubule polymerisation at the cortex. eLife 8, e50319.
Ruiz-Reig N, Chehade G, Hakanen J, Aittaleb M, Wierda K, De Wit J, Nguyen L, Gailly P, Tissir F (2022). KIF2A deficiency causes early-onset neurodegeneration. Proc Natl Acad Sci USA 119, e2209714119.
Sakakibara A, Ando R, Sapir T, Tanaka T (2013). Microtubule dynamics in neuronal morphogenesis. Open Biol 3, 130061.
Srayko M, Kaya A, Stamford J, Hyman AA (2005). Identification and characterization of factors required for microtubule growth and nucleation in the early C. elegans embryo. Dev Cell 9, 223–236.
Stepanova T, Slemmer J, Hoogenraad CC, Lansbergen G, Dortland B, De Zeeuw CI, Grosveld F, van Cappellen G, Akhmanova A, Galjart N (2003). Visualization of microtubule growth in cultured neurons via the use of EB3-GFP (end-binding protein 3-green fluorescent protein). J Neurosci 23, 2655–2664.
Subramanian R, Kapoor TM (2012). Building complexity: Insights into self-organized assembly of microtubule-based architectures. Dev Cell 23, 874–885.
Sundararajan L, Stern J, Miller DM (2019). Mechanisms that regulate morphogenesis of a highly branched neuron in C. elegans. Dev Biol 451, 53.
Tan D, Asenjo AB, Mennella V, Sharp DJ, Sosa H (2006). Kinesin-13s form rings around microtubules. J Cell Biol 175, 25.
Taylor CA, Yan J, Howell AS, Dong X, Shen K (2015). RAB-10 regulates dendritic branching by balancing dendritic transport. PLoS Genet 11, e1005695.
Thyagarajan P, Feng C, Lee D, Shorey M, Rolls MM (2022). Microtubule polarity is instructive for many aspects of neuronal polarity. Dev Biol 486, 56–70.
Tian G, Cristancho AG, Dubbs HA, Liu GT, Cowan NJ, Goldberg EM (2016). A patient with lissencephaly, developmental delay, and infantile spasms, due to de novo heterozygous mutation of KIF2A. Mol Genet Genomic Med 4, 599–603.
Tolić-Nørrelykke IM (2008). Push-me-pull-you: How microtubules organize the cell interior. Eur Biophys J 37, 1271–1278.
Trofimova D, Paydar M, Zara A, Talje L, Kwok BH, Allingham JS (2018). Ternary complex of Kif2A-bound tandem tubulin heterodimers represents a kinesin-13-mediated microtubule depolymerization reaction intermediate. Nat Commun 9, 1–13.
Tsalik EL, Niacaris T, Wenick AS, Pau K, Avery L, Hobert O (2003). LIM homeobox gene-dependent expression of biogenic amine receptors in restricted regions of the C. elegans nervous system. Dev Biol 263, 81–102.
Watabe-Uchida M, John KA, Janas JA, Newey SE, Van Aelst L (2006). The Rac activator DOCK7 regulates neuronal polarity through local phosphorylation of Stathmin/Op18. Neuron 51, 727–739.
Way JC, Chalfie M (1989). The mec-3 gene of Caenorhabditis elegans requires its own product for maintained expression and is expressed in three neuronal cell types. Genes Dev 3, 1823–1833.
Winckler B, Forscher P, Mellman I (1999). A diffusion barrier maintains distribution of membrane proteins in polarized neurons. Nat 1999 3976721 397, 698–701.
Witte H, Neukirchen D, Bradke F (2008). Microtubule stabilization specifies initial neuronal polarization. J Cell Biol 180, 619–632.
Van Beuningen SFB , Will L, Harterink M, Chazeau A, Van Battum EY, Frias CP, Franker MAM, Katrukha EA, Stucchi R, Vocking K, *et al*. (2015). TRIM46 controls neuronal polarity and axon specification by driving the formation of parallel microtubule arrays. Neuron 88, 1208–1226.
Xiao H, Verdier-Pinard P, Fernandez-Fuentes N, Burd B, Angeletti R, Fiser A, Horwitz SB, Orr GA (2006). Insights into the mechanism of microtubule stabilization by Taxol. Proc Natl Acad Sci USA 103, 10166–10173.
Yan J, Chao DL, Toba S, Koyasako K, Yasunaga T, Hirotsune S, Shen K (2013). Kinesin-1 regulates dendrite microtubule polarity in Caenorhabditis elegans. eLife 2013, 1–17.
Yogev S, Shen K (2017). Establishing Neuronal Polarity with Environmental and Intrinsic Mechanisms. Neuron 96, 638–650.
Yonekawa V, Harada A, Okada Y, Funakoshi T, Kanai Y, Takei Y, Terada S, Noda T, Hirokawa N (1998). Defect in synaptic vesicle precursor transport and neuronal cell death in KIF1A Motor protein–deficient mice. J Cell Biol 141, 431–441.
Yoshimura T, Kawano Y, Arimura N, Kawabata S, Kikuchi A, Kaibuchi K (2005). GSK-3β Regulates phosphorylation of crmp-2 and neuronal polarity. Cell 120, 137–149.
Yu W, Solowska JM, Qiang L, Karabay A, Baird D, Baas PW (2005). Regulation of microtubule severing by katanin subunits during neuronal development. J Neurosci 25, 5573–5583.
Yuen RKC, Thiruvahindrapuram B, Merico D, Walker S, Tammimies K, Hoang N, Chrysler C, Nalpathamkalam T, Pellecchia G, Liu Y, *et al*. (2015). Whole-genome sequencing of quartet families with autism spectrum disorder. Nat Med 21, 185–191.
Zhou HM, Brust-Mascher I, Scholey JM (2001). Direct visualization of the movement of the monomeric axonal transport motor UNC-104 along neuronal processes in living Caenorhabditis elegans. J Neurosci 21, 3749–3755.